JOURNAL OF PHARMACEUTICAL SCIENCES

FEBRUARY 1983
VOLUME 72 NUMBER 2

RESEARCH ARTICLES

Nonlinear Pharmacokinetics of the New Positive Inotropic Agent Sulmazole in the Dog

EDWARD R. GARRETT ˣ **and WILLY ROTH** *

Received December 14, 1981, from *The Beehive, College of Pharmacy, J. Hillis Miller Health Center, University of Florida, Gainesville, FL 32610.* Accepted for publication April 15, 1982. *Present address: Department of Biochemistry, Dr. Karl Thomae GmbH, 795 Biberach, Federal Republic of Germany.

Abstract □ Sulmazole (I) 2-[2-methoxy-4-(methylsulfinyl)phenyl]-1*H*-imidazo[4,5-*b*]pyridine, a new positive inotropic agent, is based on a pyridoimidazole nucleus. Sulmazole pharmacokinetics were monitored in plasma and urine by a specific, sensitive reverse-phase fully automated HPLC system with fluorimetric detection. The hydroxylated metabolite, III, was also monitored in the urine, and unusual pharmacokinetics were observed. Sulmazole disappeared and metabolite II appeared in plasma by zero-order rates for most of their time courses in the 2–15-mg/kg range with a 75% conversion to II. Pure Michaelis–Menten pharmacokinetics were not applicable, and the v_{max} value increased with increasing dose. Pharmacokinetics of sulmazole and II at 0.7-mg/kg iv doses were characterized by a first-order two-compartment body model. Metabolite III at 0.7- and 2-mg/kg iv doses showed no dose-dependent pharmacokinetics. The unchanged drug and its major metabolite, II, were negligibly excreted renally (0.5–2%). Their renal clearance showed urine flow rate dependencies. The plasma protein bindings were: sulmazole, 40.8 ± 1.0%; II, 54 ± 2%; III, 43 ± 1%, and they were concentration independent.

Keyphrases □ Pharmacokinetics—nonlinear, sulmazole, in the dog □ Models, pharmacokinetic—nonlinear, sulmazole, in the dog □ Sulmazole—nonlinear pharmacokinetics in the dog

Sulmazole[1] (I) has shown positive inotropic activity in an isolated dog heart preparation and in intact dogs (1–4). The onset and magnitude of cardiovascular response of this new nonglycosidic cardiotonic drug was studied in humans (5–10). The drug's action started immediately after intravenous administration, indicating that action was due to the parent compound (5) on the presumption that the time course of pharmacological action was related to the time course of the active drug in the central circulation.

Pharmacokinetic studies of radiolabeled I have been conducted in the rat (11, 12), baboon (13), rabbit and dog (14), and rhesus monkey (15), but only total radioactivity was measured. These studies did not reveal the pharmacokinetic behavior of the extensively metabolized I (16).

The present paper reports on the pharmacokinetics of I as a function of dose using specific and sensitive high-performance liquid chromatographic (HPLC) assays (17, 18). The stability, protein binding, and red blood cell partitioning of I, administered intravenously in dogs, and its metabolites, excreted in the urine, were also studied. Various methods of challenging the possible Michaelis–Menten pharmacokinetics of sulmazole were developed and applied to the data.

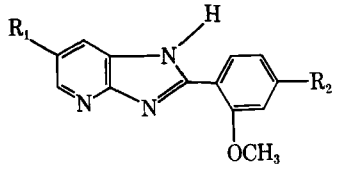

Compound	R_1	R_2	Name
I	H	$-SOCH_3$	2-[2-methoxy-4(methylsulfinyl)-phenyl]-1*H*-imidazo[4,5-*b*]pyridine; Sulmazole[1], mol. wt. 287.3
II	H	$-SO_2CH_3$	2-[2-methoxy-4-(methylsulfonyl)-phenyl]-1*H*-imidazo[4,5-*b*]pyridine[2] mol. wt. 303.3
III	OH	$-SOCH_3$	6′-hydroxy-2-[(2-methoxy-4-methylsulfinyl)phenyl]-1*H*-imidazo[4,5-*b*]pyridine; metabolite M2; mol. wt. 303.3

[1] AR-L 115 BS, Lot No. Ch.-B 00718, Dr. Karl Thomae GmbH, 7950 Biberach/Riss, West Germany.

0022-3549/83/0200-0105$01.00/0

EXPERIMENTAL

Materials—Sulmazole, 2-[2-methoxy-4-(methylsulfinyl)phenyl]-1*H*-imidazo[4,5-*b*]pyridine, I, was obtained in ampules of 1000 mg/10 ml[1]. Synthesized (19) ^{14}C-I had >99% chromatographic purity by TLC with subsequent liquid scintillation counting of extracted material and by radioscanning. This purity was substantiated by HPLC analysis. Reference compounds II and III were also obtained[2]. The solvents and reagents used were anhydrous dibasic sodium phosphate[3], 85% phosphoric acid[4], acetonitrile HPLC grade[4], 30% hydrogen peroxide[4], and phenobarbital sodium USP XIV granular[5]. A toluene base scintillation fluid[6] was used for the radioactive counting with a liquid scintillation counter[7]. Standard catheters were used for catheterization of the jugular[8] and the foreleg[9] veins. Blood was withdrawn into heparinized containers[10].

Pharmacokinetic Studies in Dogs—Three healthy male mongrel dogs (23–27 kg) were used for the pharmacokinetic investigations. Their blood analysis showed no pathogenic abnormality or presence of microfilaria. The dogs were fasted at least 17–20 hr before each study and were given water *ad libitum*. The animals were supported by a dog sling in a frame[11] placed on a laboratory table. The dogs were given 120 ml of water, 30–45 min prior to the experiments, followed by intravenous saline infusion (35 drops/min) until drug administration when the intravenous drip was reduced to 20 drops/min. One day before the experiment, the animals were catheterized with a 30.5-cm standard catheter in the jugular vein after local anesthesia with mepivacaine hydrochloride[12]. A second catheter was also implanted in a foreleg vein (vena brachialis). On the following day, the drugs were injected directly into the jugular catheter (1–4 sec) followed by flushing of the catheter with 20 ml of physiological saline. Then, the catheter was connected by a three-way stopcock[13] to the saline infusion bottle[14]. Blood samples (4 ml) were taken into a heparinized vacutainer[10] after filling the dead volume of the catheter with blood by aspirating with an extra syringe. These samples were discarded. During the first hour, blood was taken from the foreleg vein with subsequent sampling from the jugular. In several studies, samples were taken simultaneously from both sites in the first hour. The heparinized blood was centrifuged immediately for 5–8 min at 3000 rpm, and plasma was removed with sterile glass pipets. The red blood cells were suspended in 2 ml of physiological saline and stored in an ice bath for reinfusion at the end of the study. Plasma was injected directly and immediately into an HPLC system after appropriate dilution and recentrifugation. Urine was collected from the dogs through a urinary catheter[15] at 15–30-min intervals up to 10–24 hr. Withdrawal time, volumes, and urinary pH were recorded, and aliquots of each sample were frozen until analyzed.

One 24-kg dog, previously studied at several intravenous doses, was administered orally 16 mg/kg/day of phenobarbital in gelatin capsules[8] for 13 days. Subsequently, the pharmacokinetics of an intravenous bolus of 2 mg/kg of I were studied in this dog.

HPLC Assays—A fully automated HPLC system (18) permitted the direct injection of body fluids. The drugs and metabolites were trapped on either of two alternately working enrichment precolumns and dry-filled with reverse-phase material[16], while nonlipophilic material was separated by flushing the precolumns for 3 min with deionized water with a 2-ml/min flow rate. Backflush elution with the mobile phase was used to desorb the drugs from the precolumns to the analytical column in order to chromatographically separate and quantify. The equipment consisted of an autosampler[17], two HPLC pumps[18], a fluorescence detector[19], a chromatographic data station[20], and a self-made precolumn switching system activated by pressurized air (18). The mobile phase for I and II was acetonitrile–0.05 *M* dibasic sodium phosphate buffer (1:2.3, mobile phase A) apparent pH 6.8, with respective retention times of 2.40 and 3.01 min. The mobile phase for III (mobile phase B) had a retention time of 5.74 min and was mobile phase A diluted 1:1.13 with deionized water when urine was assayed after administration of I. When III was administered intravenously, there were no interferences at its 2.03-min retention time, and mobile phase A was used. A self-packed steel column[21] with reverse-phase material[22] was used with a working pressure of 8.5 megapascals at 49° (flow rate: 2 ml/min for mobile phase A; 2.5 ml/min for mobile phase B). The wavelengths (excitation/emission) in urine and plasma were 330 and 370 nm for compounds I and II and 345 and 515 nm for III. These wavelength selections permitted no mutual interferences of III with I and II. The slit width was adjusted to 10 nm (excitation) and 5 and 10 nm (emission) for I, II, and III, respectively. Calibration curves were established in the biological fluid as concentration *versus* peak area (19).

Stability Studies—Solutions of ~100 and 1000 ng/ml of I, II, and III were prepared in 1.0 *N* NaOH[23] and 1.0 *N* HCl[23], and the concentrations were monitored by specific HPLC assay after 0, 4, and 20 hr at 20 and 47°. Similar studies were conducted in fresh dog plasma and urine at 20 and 37.5°.

Protein Binding—Protein binding was studied by ultrafiltration (20) and ultracentrifugation in freshly prepared dog plasma obtained by centrifugation of heparinized dog blood (5000 U of heparin[24]/50 ml of blood) for 20 min at 2000 rpm. [^{14}C]-I and metabolites II and III were used.

Ultrafiltration—Ultrafiltration membrane cones[25] were immersed for 5 hr in refrigerated deionized water, and excess liquid was removed by centrifugation for 5 min at 1000 rpm. Since I showed markedly unspecific binding to the filter cones in the range of 17.6–33% at concentrations of 3.5×10^{-3}–3.5×10^{-5} *M*, all cones were presaturated with appropriate concentrations prior to the experiment, which reduced the unspecific binding to 0–4.3% (20). The fraction bound was calculated from the HPLC and liquid scintillation counting assay of the total concentration prior to the ultrafiltration of 2.5–3 ml of plasma and in the plasma water filtrate after 30% filtration.

Ultracentrifugation—Drug concentrations between 10^{-6} and 10^{-8} *M* in dog plasma were centrifuged[26] for 20 hr at 45,000 rpm at 20°. Initial and supernatant concentrations were determined by liquid scintillation counting for I and by HPLC for I, II, and III.

Red Blood Cell Partitioning—The time dependency of red blood cell partitioning of I (1.02 μg/ml) was investigated in prepared heparinized dog blood with a previously determined hematocrit. The blood (5 ml) was maintained at 37.5°, and 200-μl aliquots were removed at 2-min time intervals and digested for 5 hr with 2 ml of a mixture of 2-propanol[4]–commercial solvent[27] (1:1.5). Decoloration was effected with 0.2 ml of hydrogen peroxide for 30 min, then 10 ml of scintillation fluid[6] was added. After an adaptation period of 6 hr at 10°, liquid scintillation counting was performed. The centrifuged plasma was assayed similarly, and the red blood cell–plasma water partition coefficients were determined similarly. Freshly prepared red blood cells, obtained by centrifugation of heparinized dog blood at 1500 rpm, were washed four times with plasma water with subsequent centrifugation and were then resuspended in plasma water. They were also resuspended in iso-osmolar physiological buffer (5.52 g of Na_2HPO_4, 0.86 g of KH_2PO_4, and 32 g of NaCl/liter). The hematocrit was determined and the suspension was spiked with eight different concentrations of I in the range of 9.8×10^{-6}–9.6×10^{-8} *M*. After 20 min of incubation at 37.5° under gentle mixing, aliquots were taken, the hematocrit determined, and the partition coefficient calculated (21).

RESULTS AND DISCUSSION

HPLC Assays—The described automated system permits direct injection of urine and plasma (diluted at least 1:1.5 with deionized water) from an automatic injection system for assays of I, II, and III. The sample adsorbed on the reverse-phase material of the precolumn was washed

[2] AR-L 114 BS, DR. Karl Thomae GmbH, 7950 Biberach/Riss, West Germany.
[3] Mallinckrodt, Inc., Paris, KY 40361.
[4] Fisher Scientific Co., Fair Lawn, NJ 07410.
[5] Mallinckrodt Chemical Works, St. Louis, MO.
[6] Scinti-Verse, Fisher Scientific Co., Fair Lawn, NJ 07410.
[7] Packard Tri Carb 460 CD Liquid Scintillation System, Packard Instrument Co. Inc., Downers Grove, IL 60515.
[8] Intracath intravenous catheter placement unit 30.48 cm (12 in), 16 gauge, The Deseret Co., Sandy, UT 84070.
[9] 30.48 cm (12 in) catheter, 17 gauge 0.031 in. i.d., The Deseret Co., Sandy, UT 84070.
[10] Becton Dickinson Vacutainer, heparinized, Rutherford, NJ 07070.
[11] Alice King Chatham Medical Arts, Los Angeles, CA 90043.
[12] Carbocaine, Winthrop Laboratories, New York, NY 10016.
[13] Pharmaseal, Toa Alta, PR 00758.
[14] McGaw Laboratories, Irvine, CA 92714.
[15] Monojet, Division of Sherwood Co., A Brunswick Co., St. Louis, MO 63103.
[16] Bondapak C_{18}-Corasil, Waters Associates, Milford, MA 01757.
[17] Model 420B, Perkin-Elmer, Norwalk, CT 06856.
[18] Series 3B, Perkin-Elmer, Norwalk, CT 06856.
[19] Model 650S, Perkin-Elmer, Norwalk, CT 06856.
[20] Data Station Sigma 15, Perkin-Elmer, Norwalk, CT 06856.
[21] Herbert Knauer, 6370 Ober Ursel, West Germany.
[22] Hypersil ODS particle size 5 μm, Shandon Southern Products, United Kingdom, Astmore, Runcorn WA 71 PR.
[23] Ricca Chemical Co., Arlington, TX 76012.
[24] Heparin Sodium, 10,000 U/ml, The Upjohn Co., Kalamazoo, MI 49001.
[25] Membrane filter cones 2100 CF 50, Amicon Co., Lexington, MA 02173.
[26] Beckman Ultracentrifuge model LS-50 with rotor Ti 50, Beckman Instruments, Norcross, GA 30092.
[27] Biosolv, Beckman Inc., Fullerton, CA 92634.

for 3 min with deionized water to remove water soluble substances in the plasma and urine. Subsequently, the mobile phase backflushed the adsorbed material into the analytical column for HPLC assay, and the printer-plotter was activated to record the chromatogram 3 min after injection on the precolumn. The automated system of switching valves permitted injection and flushing of water soluble substances on one precolumn, while the second precolumn was backflushed for assay. The total time for a single assay was 12–15 min and 64–80 assays can be performed automatically in an 8-hr period.

In the assays of I (2.40 min) and II (3.01 min) in urine with mobile phase A, a peak due to an unknown metabolite was observed at 2.20 min that did not interfere with these fluorimetric assays at 330-nm excitation and 370-nm emission. In the assay of III (5.74 min) in dog urine with mobile phase B, peaks due to unknown metabolites were observed at 2.21, 3.63, 6.85, and 9.05 min with the fluorimetric assay at 345-nm excitation and 515-nm emission. These peaks did not appear in blank urine when III was administered intravenously, and mobile phase A could be used for a retention time of 2.03 min at 345-nm excitation and 515-nm emission.

The regression statistics (22) of calibration curves (n = 13–27) of concentrations *versus* peak area in the range of 20–1000 ng/ml for I and II and 40–1000 ng/ml for III gave analytical sensitivities (2 times the standard error of the estimate of concentration on peak area) of 15–18 ng/ml for plasma and 12–26 ng/ml for urine. All curves showed intercepts not significantly different from zero, correlation coefficients >0.990, standard errors of regression coefficient of 0.4–0.9% of the coefficient, and standard errors of the intercept within ±4.1 ng/ml.

Protein Binding—Plasma protein binding percentages (percent of 100 times the concentration in plasma–water/concentration in plasma) for different concentrations of drug and metabolites showed no apparent dose dependencies of protein binding. The percent protein bindings of I in the plasma concentration range of 50–15,000 ng/ml were consistent by both ultrafiltration (41.5 ± 1.2%, n = 6) and ultracentrifugation (40.5 ± 1.5%, n = 11) techniques, and the overall average was 40.8 ± 1.0% (*SEM*). The percent protein binding of II and III were 54 ± 2% (n = 3) and 43 ± 1% (n = 3), respectively, as determined by the ultracentrifugation technique in the 140–1500-ng/ml plasma range.

Red Blood Cell–Plasma Water Partitioning—The red blood cell–plasma water partition coefficient is the ratio of concentrations in the red blood cell to that in the plasma water. It can be calculated from the drug concentrations in plasma before and after equilibration with red blood cells with a known hematocrit, $H = V_{RBC}/V_{blood}$, and when the fraction, f, of the drug bound to plasma proteins is known, by means of an equation developed previously (21, Eq. 9). The time-dependent studies showed that red blood cell–plasma equilibration was achieved within 10 min (n = 7), since there was no significant difference in radioactivity counts of the supernatant, 2246 ± 36 cpm/ml (*SD*) of plasma water after that time. The partition coefficients, D, calculated from studies in whole blood and for red blood cells suspended in plasma–water showed no significant dose dependencies. The calculated partition coefficients averaged 3.10 ± 0.05 (*SEM*) in whole blood in the range of 67–6000 ng/ml (n = 6) and 2.72 ± 0.30 in red blood cell suspensions in plasma water in the range of 28–2820 ng/ml (n = 7). There was no significant difference when physiological buffer was used for the red blood cell suspensions. At 157 ng/ml, D was 3.20 ± 0.09 and 3.10 ± 0.13 from plasma–water and buffer, respectively.

Studies at 200 ng of I/ml also were conducted with the use of the HPLC assay for nonradiolabeled compound, where D = 2.59 for 6.9×10^{-7} M in blood and 5.52×10^{-7} M in plasma and D = 2.07 for 200 ng/ml in the red blood cell suspension and 140 ng/ml in the plasma water.

Stability of Compounds—The concentrations from the HPLC assays of I after appropriate dilution when subjected to 1.0 N NaOH and 1.0 N HCl for 20 hr were no different than when assayed at time zero. The maximum decrease in concentrations of I, II, and III at 100 and 1000 ng/ml of fresh dog plasma after 24 hr at 37.5° was 4 and 0.5% for I; 0.0 and 0.1% for II; and 0.1 and 0.0% for III. The values were the same when the samples were incubated in fresh dog urine. Thus, there was no significant degradation within 1 day for I, II, and III in strong acid, strong alkali, or in plasma or urine.

Nonlinear Plasma Pharmacokinetics of Sulmazole: Data Analysis on the Presumption of Michaelis–Menten Kinetics—The semilogarithmic plots of plasma levels of I *versus* time (Fig. 1) are given for several studies at different doses in dogs. Data was obtained from blood taken from the foreleg vein during the first hour and from the jugular after that. The concentrations of sulmazole in jugular blood were up to 3.0 times higher than that of foreleg blood in the first 15 min during the 2 mg/kg iv study in dog 1. Subsequently, the values coincided. The S-shapes of such curves are indicative of primarily saturable elimination processes

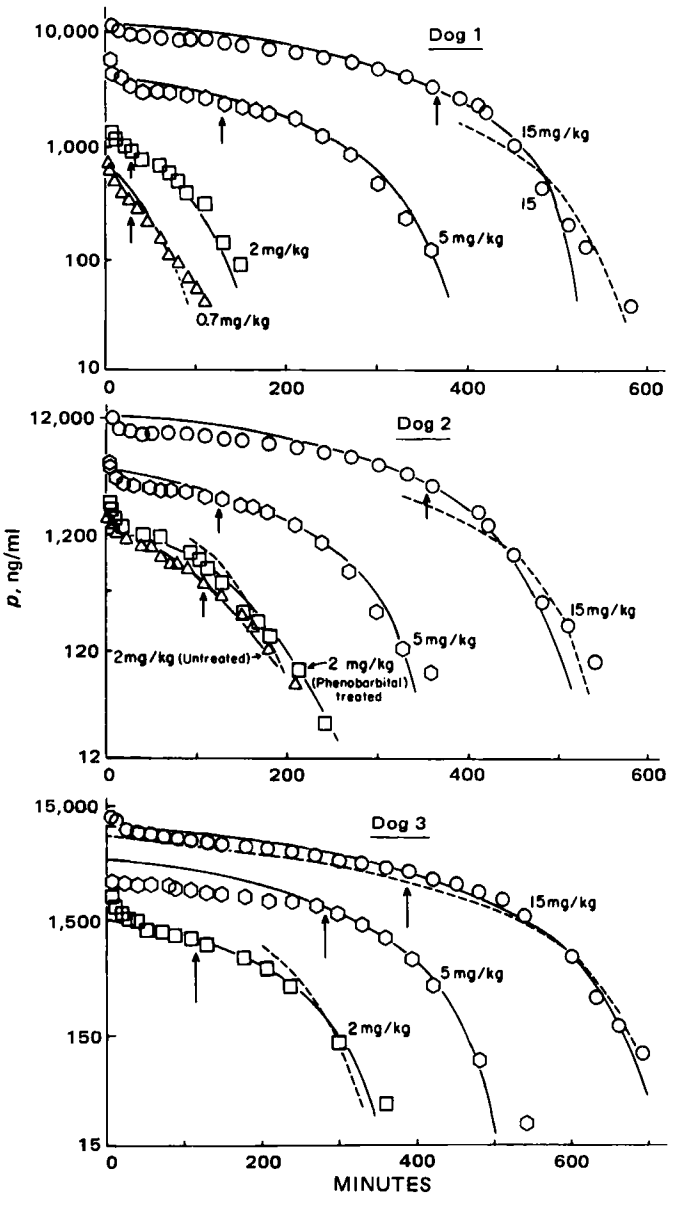

Figure 1—*Semilogarithmic plots of plasma levels of sulmazole on intravenous bolus administration of the labeled dose to dogs. The solid curves through the experimental values were calculated by Eq. 6 from the parameters given in Table I for each dog study. The squared symbols for dog 2 are for a study at 2 mg/kg after the dog had been treated daily with 16 mg/kg of oral phenobarbital over 13 days. The dashed lines for each dog study were plotted by Eq. 6 using the parameters for the 5-mg/kg dose study for each dog (Table I). The arrows designate the plasma level (p_1) values taken at time t_1 for the calculation of t_2 for any plasma level p_2. The initial estimation of Michaelis–Menten parameters by application of Eq. 5 were made from paired values subsequent to that time, t_1.*

in the disposition phase (23). The initial sharp decrease can be assigned to distribution and the subsequent increasing slopes with time to disposition. If there were only one saturable process and no significant parallel first-order elimination, the rate of plasma concentration (p) decrease subsequent to equilibration of the drug in the body would be characterized by:

$$-dp/dt = \frac{v_{max}\, p}{K_m + p} \qquad \text{(Eq. 1)}$$

where v_{max} is the maximum possible rate of decrease of plasma concentration (ng/ml/min) at maximal plasma levels, and v_{max}/K_m is the apparent first-order rate constant for terminal first-order elimination of drug when plasma levels approach zero:

$$\lim_{p \to \infty} -dp/dt = v_{max} \qquad \text{(Eq. 2)}$$

Table I—Parameters for Apparent Nonlinear Pharmacokinetics of Sulmazole and the Formation of Its Major Metabolite II

Parameter	Dog 1			Dog 2			Dog 3			Averages[a]			Overall average[a]
Weight, kg	22.4	25.4	23.4	25.4	25.0	24.6	26.5	25.2	25.0				
Dose, mg (mg/kg)	336(15)	127(5)	46.8(2)	381(15)	125(5)	49.2(2)	398(15)	126(5)	50(2)	(15)	(5)	(2)	
v_{max}[b], ng/ml/min	23.9 ± 0.6	12.8 ± 0.8	10.9 ± 0.4	30.8 ± 1.3	13.9 ± 1.0	10.4 ± 1.0	17.2 ± 0.6	13.1 ± 0.8	4.9 ± 0.3	23.9 ± 3.9	13.3 ± 0.3	8.7 ± 1.9	15.3 ± 2.6
$10^3 v_{max}/K_m$[b], min^{-1}	153 ± 65	73 ± 31	48 ± 3	79 ± 19	88 ± 45	33 ± 3	47 ± 7	54 ± 12	74 ± 63	93 ± 31	72 ± 10	52 ± 12	72 ± 12
$(t_{1/2})v_{max}/K_m$, min	4.5 ± 1.5	9.5 ± 3.4	14.5 ± 1.0	8.8 ± 2.0	7.8 ± 3.0	21.1 ± 1.0	14.7 ± 2.2	12.8 ± 3.6	9.3 ± 5.0	9.7 ± 1.5	10.0 ± 1.5	15.0 ± 3.4	11.4 ± 1.6
K_m[c], ng/ml	156 ± 60	175 ± 67	228 ± 24	391 ± 107	157 ± 85	313 ± 51	364 ± 68	242 ± 66	66 ± 35	304 ± 74	191 ± 26	202 ± 72	232 ± 36
k_0^I/V_I[d], ng/ml/min	20.8	11.0	8.0	23.6	12.1	6.4	12.7	5.1	4.5	19.0 ± 3.3	8.9 ± 1.9	6.3 ± 1.0	11.4 ± 2.2
V_I[e], liters	31.4	32.6	36.0	31.7	34.7	42.8	46.0	40.0	33.3	36.4 ± 4.8	35.8 ± 2.2	37.4 ± 2.8	36.5 ± 1.7
V_I'[f] liters	40.0	43.8	42.5	43.5	41.7	39.4	44.5	40.0	33.3	42.7 ± 1.4	41.8 ± 1.1	38.4 ± 2.7	41.0 ± 1.1
k_0^I[g], ng/min	6.53	3.58	2.88	7.48	4.21	2.74	5.84	2.04	1.50	6.62 ± 0.48	3.10 ± 0.53	2.37 ± 0.44	4.03 ± 0.70
$(k_0^I)'$[h], ng/min	8.32	4.81	3.40	10.26	5.05	2.52	5.65	2.04	1.50	8.08 ± 1.34	3.97 ± 0.97	2.47 ± 0.55	4.92 ± 0.88
10^{-3} AUC_∞^I/dose[i], (ml/min)/(mg/kg)	177	134	42	260	120	56	200	177	130	213 ± 25	144 ± 17	76 ± 27	144 ± 23
k_0^{II}/V_{II}[j], ng/ml/min	11.14	6.48	11.06	11.02	8.22	11.14	9.20	3.13	2.02	10.45 ± 0.63	5.94 ± 1.49	8.07 ± 3.03	8.16 ± 1.19
10^3 Cl^{II}/V_{II}[j], min^{-1}	4.0	6.7	39.7	6.2	12.7	4.0	7.5	4.5	4.6	5.9 ± 1.0	8.0 ± 2.5	16.1 ± 11.8	10.0 ± 3.8
10^3 β_{II}[k], min^{-1}	29.0	27.1	24.6	24.7	24.7	25.1	34.3	26.6	22.2	29.3 ± 2.8	26.1 ± 0.7	24.0 ± 0.9	26.5 ± 1.2
$(t_{1/2})\beta_{II}$[k], min	23.4	25.6	28.2	28.0	28.0	27.7	20.2	26.0	31.1	23.9 ± 2.3	26.5 ± 0.7	29.0 ± 1.1	26.5 ± 1.1
C_0^{II}[k], ng/ml	1.02×10^9	1.77×10^6	5.01×10^3	5.24×10^7	4.16×10^5	1.30×10^4	1.08×10^{12}	3.49×10^7	1.16×10^5				
k_0^{II}[l], ng/min	5.41	3.15	5.37	5.35	3.99	5.41	4.46	1.52	0.981	5.07 ± 0.31	2.89 ± 0.73	3.92 ± 1.47	3.96 ± 0.58
$k_{0_{corr}}^{II}/k_0^I$[m]	0.783	0.834	(1.77)	0.677	0.898	(1.87)	0.724	0.706	0.620	0.728 ± 0.031	0.813 ± 0.056	(1.42 ± 0.4)	0.749 ± 0.036
10^{-3} AUC_∞^{II}/dose of I[n], (ml/min)/(mg/kg)	47.7	37.0	17.5	34.7	28.6	22.3	38.4	36.4	31.0	40.3 ± 3.9	34.0 ± 2.7	23.6 ± 4.0	32.6 ± 3.0

[a] The ± values for the averages are the *SEM* for the values averaged. [b] $1/v_{max}$ and K_m/v_{max} values were determined from the slopes and intercepts, respectively, of the statistical regression of $(t_2 - t_1)/\ln(p_1/p_2)$ against $(p_1 - p_2)/\ln(p_1 - p_2)$ in accordance with Eq. 5 for all pairs of I plasma levels, p_1 and p_2, at their respective times, t_1 and t_2, in the postdistributive phases. The correlation coefficients ranged between 0.9559 and 0.9888. The values of v_{max} and v_{max}/K_m and their error estimates were calculated from the respective reciprocals of the slope ± s slope, and of the intercept ±s intercept. [c] Intercept, K_m/v_{max}, divided by slope, $1/v_{max}$. [d] Best estimate of slope of plasma level of I against time on the presumption of zero-order kinetics in the disposition phase. [e] $V_I = D_0/C_0$ where D_0 is dose of I in milligrams and C_0 is the extrapolated intercept of the estimated zero-order loss, k_0^I/V_I (ng/ml/min). [f] $V_I = D_0/C_0$ where C_0 was obtained from the extrapolated intercept of a line through the plateau values in the 40–100-min interval (Fig. 3) after intravenous administration. [g] $k_0^I = V_I \times k_0^I/V_I$. [h] $(k_0^I)' = V_I \times k_0^I/V_I$. [i] Total area (ng/ml/min) under plasma level–time curve of I per mg/kg of I dose. [j] The apparent zero-order rates of formation of II, k_0^{II}/V_I, and its subsequent clearance per unit volume, Cl^{II}/V_{II}, were determined from the respective slopes and intercepts of plots (Fig. 7) in accordance with Eq. 16. [k] Parameters for first-order elimination of II after cessation of formation from I in accordance with $C_0^{II} = e^{-\beta_{II}t}$ where C_0^{II} is the extrapolated value to zero time. [l] Nanograms of II formed/min from I calculated from $V_{II}(k_0^{II}/V_{II})$ where V_{II} was taken as the 48,558-ml apparent overall volume of distribution determined from the study after administration of 0.7 mg/kg iv of II. [m] Fraction of rate of loss of I transformed to II, *i.e.*, $k_0^{II}(corr)/k_0^I = (k_0^{II}/k_0^I)$ mol. wt. I/mol. wt. II = 0.9473 (k_0^{II}/k_0^I). The overall average is given with the values for 2-mg/kg doses in dogs 1 and 2 omitted. [n] AUC_∞^{II} is by trapezoidal rule of area under plasma level of II *versus* time on intravenous administration of I plus $[II]_n/\beta_{II}$ where $[II]_n$ is the terminal plasma level at t_n used to estimate $AUC_{t_n}^{II}$ up to that time. This value is divided by the dose of I (mg/kg).

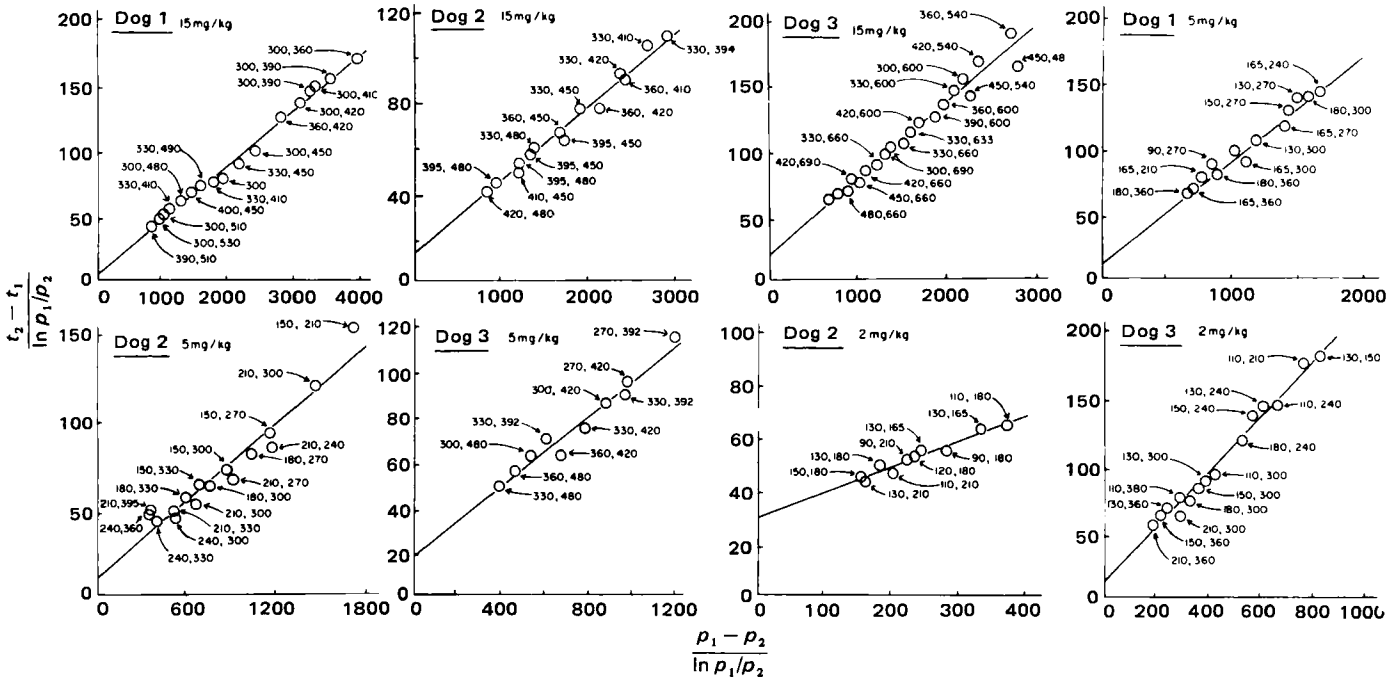

Figure 2—*Plots of paired sulmazole plasma level–time data after the time given by the arrow in Fig. 1 in accordance with Eq. 5 to estimate* $1/v_{max}$ *from the slope and* K_m/v_{max} *from the intercept. Each data point is labeled with the times after administration of the data pair used (*p_1 *at* t_1 *and* p_2 *at* t_2*).*

and

$$\lim_{p \to 0} -dp/dt = (v_{max}/K_m)p \qquad \text{(Eq. 3)}$$

If the elimination process can be attributed to saturable metabolism, K_m can be interpreted as the affinity constant for the available enzymes where the metabolic rate is proportional to the amount of drug–enzyme complex. When all enzymes are complexed in the steady state, the maximal zero-order rate, v_{max}, would be achieved. The data for all doses appeared to approach a final first-order loss of drug from the plasma (Fig. 1) with visually estimated apparent half-lives of 30.0 ± 5.9 (*SD*) ± 2.9 min (*SEM*) for dog 1 (n = 4), 27.2 ± 7.0 (*SD*) ± 4.0 min (*SEM*) for dog 2 (n = 3), and 30.8 ± 1.0 (*SD*) ± 0.6 min (*SEM*) for dog 3 (n = 3).

These estimates of the terminal half-lives are approximate and likely overestimate $0.693/(v_{max}/K_m)$, since they may be based on an estimated linearity of a slightly curving semilogarithmic plot of the terminal plasma concentrations against time (Fig. 1).

The saturable disposition phase after complete equilibration of the drug among the tissues of the body can be characterized by the integrated form (24) of Eq. 1:

$$(p_1 - p_2) - K_m \ln \frac{p_2}{p_1} = v_{max}(t_2 - t_1) \qquad \text{(Eq. 4)}$$

where p_1 and p_2 are plasma concentrations in the postdistribution phase taken at times t_1 and t_2, respectively. This transcendental equation has no explicit solution for plasma concentration with time. Equation 4 can be rearranged to:

$$\frac{t_2 - t_1}{\ln (p_1/p_2)} = \frac{p_1 - p_2}{\ln (p_1/p_2)} \frac{1}{v_{max}} + \frac{K_m}{v_{max}} \qquad \text{(Eq. 5)}$$

where $1/v_{max}$ and K_m/v_{max} are the respective slopes and intercepts that can be estimated from linear plots of $(t_2 - t_1)/\ln(p_1/p_2)$ against $(p_1 - p_2)/\ln(p_1/p_2)$ for any pair of plasma levels, p_1 and p_2, at their respective times, t_1 and t_2, in the postdistributive phase. Examples of such plots are given in Fig. 2 and the resulting calculated values of K_m and v_{max} are listed in Table I. Such plots must be restricted to plasma levels subsequent to the achievement of pseudo steady-state equilibration among the tissues of the body, *i.e.*, the establishment of a one-compartment body model. Also, they are only valid for estimation of parameters (Table I) when there is only one saturable elimination process and no significant amount of drug is eliminated by any parallel first-order process. Thus, p_1-values were not taken at earlier times. The p_1-values, taken after body equilibration of drug was assumed (arrows in Figs. 1 and 3), were then paired with later p_2-values, not too close in time, to produce the plots of Fig. 2 in accordance with Eq. 5. The v_{max}- and K_m-values were then substituted into a rearranged Eq. 4:

$$t_2 = \frac{p_1 - p_2}{v_{max}} - \frac{K_m}{v_{max}} \ln \frac{p_2}{p_1} + t_1 \qquad \text{(Eq. 6)}$$

An experimental value for p_1 at a known time t_1 (designated by the arrows in Figs. 1 and 3) in the presumed pseudosteady-state phase was assumed to be valid, and t_2-values were calculated for various p_2-values. The solid curves in Fig. 1 and the dashed curves in Fig. 3 were calculated in this manner.

Although the parameters v_{max} and K_m (Table I) for Eqs. 4 and 6 obtained in this manner permit good fit to the experimental plasma level–time data (Figs. 1 and 3) subsequent to the time when pseudo steady-state equilibrations among body tissues are probably established, the calculated plasma level values significantly overestimate the experimental values in the early time periods subsequent to the usual relatively rapid (α-phase) tissue distribution.

Table II—Parameters for Apparent Linear Pharmacokinetics of Sulmazole and Metabolites II and III in the 24.2-kg Dog 1

Parameter	Compound I	II	III	
Dose, mg/kg	0.7	0.7	1.0	2.0
mg	16.94	16.73	24.4	48.8
a^a, ng/ml	325	500	2000	4600
b^a	573	302	272	552
α^a, min^{-1}	0.384	0.384	0.221	0.271
($t_{1/2}$, min)	(1.80)	(1.81)	(3.13)	(2.56)
β^a	0.0235	0.0326	0.0186	0.0186
	(29.5)	(21.2)	(37.3)	(37.3)
$Cl_{tot}{}^b$, ml/min	671	1583	1031	1046
$Cl_{ren}{}^c$	13.9	3.00	0.25	0.25
$Cl_{met}{}^d$	657	1580	1031	1046
$V_c{}^e$, liters	18.9	20.9	10.7	9.5
$V_d{}^f$	28.6	48.6	55.5	56.2
$V_{extrap}{}^g$	29.6	55.4	9.0	8.8

[a] Parameter description of time course of plasma concentrations, $p = ae^{-\alpha t} + be^{-\beta t}$. [b] $Cl_{tot} = AUC_\infty$/dose (ng) where the total area under the plasma level–time curve is $AUC_\infty = A/\alpha + b/\beta$. [c] Slope of plot of cumulative drug *excreted at time* t, ΣU_t, against the area under the plasma level–time curve until that time, where $AUC_t = (a/\alpha)(1 - e^{\alpha t}) + (b/\beta)(1 - e^{-\beta t})$. [d] $Cl_{met} = Cl_{tot} - Cl_{ren}$. [e] Apparent volume of distribution of central compartment referenced to plasma concentration, $V_c = p_0$/dose (ng) = $(a + b)$/dose (ng). [f] Apparent overall pseudo steady-state volume of distribution referenced to plasma concentration, $V_d = Cl_{tot}/\beta$. [g] Apparent overall volume of distribution on the assumption of the one-compartment body model, V_{extrap} = b/dose (ng).

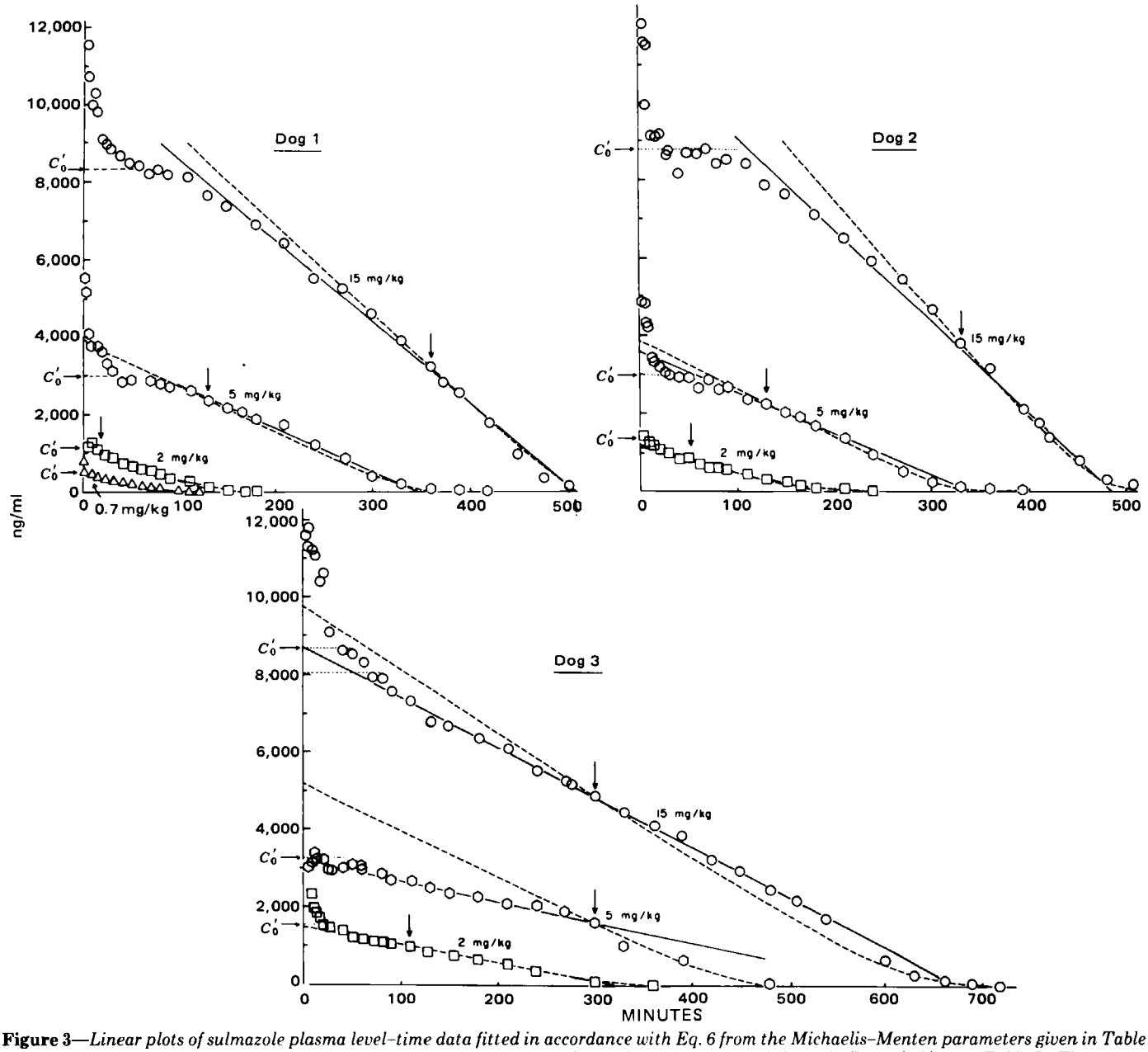

Figure 3—*Linear plots of sulmazole plasma level–time data fitted in accordance with Eq. 6 from the Michaelis–Menten parameters given in Table I (- - -) and fitted on the presumption of constant zero-order rates of plasma level decay (—) of slopes* k_0/V *(ng/ml/min) (Table I). The arrows designate the plasma level* (p_1) *values taken at time* t_1 *for the calculation of* t_2 *for any plasma level* p_2 *by Eq. 6.*

This can be seen at the 15-mg/kg dose but less so at the 2-mg/kg dose. One possible explanation of the constantly recurring plateau or increase in plasma levels for all three dogs at 40–100 min after drug administration may be the presence of enterohepatic recirculation, the delayed continuous reabsorption of biliary excreted sulmazole from the GI tract.

The v_{max}-values of Table I have reasonable precision that average ±7% and show a decided dose effect: 23.9 ± 3.9, 13.3 ± 0.3, and 8.7 ± 1.9 ng/ml/min (*SEM*) at the 15-, 5-, and 2-mg/kg iv doses of sulmazole, respectively. The estimated K_m-values with their much higher variability averaging ±32% do not permit any conclusion as to dose dependencies. The overall average of 232 ± 36 ng/ml (*SEM*) is relatively small and does not disturb the linearities of the concentration–time plots of sulmazole for the greatest portion of the time course.

The fact that one set of v_{max}/K_m-values fails to characterize the plasma level–time values of sulmazole for all doses is apparent when the set of values for the 5-mg/kg dose was used to attempt to fit the data at all doses (dashed lines in Fig. 1).

The v_{max}/K_m-values and the derived $(t_{1/2})_{v_{max}}/K_m$-values (Table I) provide estimates of the apparent first-order rate constant effective at low drug concentrations in plasma in accordance with the postulation of one saturable elimination process directing the elimination that conforms to Michaelis–Menten kinetics.

Although there appears to be a systematic decrease in the averages of the v_{max}/K_m-values and an accompanying systematic increase in the averages of the apparent half-lives with decreasing dose (0.7 ± 1.5, 10.0 ± 1.5,and 15.0 ± 3.4 min (*SEM*) at 15, 5, and 2 mg/kg of sulmazole, respectively), the standard errors do not permit an absolute decision. The data for dog 3 were contrary to those of the averages.

The plasma level–time curve for sulmazole at the lowest dose studied, 0.70 mg/kg, is plotted semiliogarithmically in Fig. 4. At this dose the pharmacokinetics appear to be linear; the drug appears to be eliminated by first-order processes from a two-compartment body model. The pharmacokinetic parameters are listed in Table II. The terminal half-life of 29.5 min confirms the indicated increase of the terminal half-life with decreasing dose.

Data Analyses on the Presumption of Zero-Order Pharmacokinetics—Constant slopes k_0^I/V_I (ng/ml/min) can be obtained from the slopes of the plotted data in Fig. 3 and can reasonably characterize the plasma level–time data of sulmazole. These are given in Table I and are close to the estimated v_{max}-values. Considering that they give less weight to the terminal data, they show similar dose dependencies.

The dose dependencies of k_0/V_I and v_{max} permit the conclusion that the simple model of a Michaelis–Menten single saturable elimination process with a constant v_{max} cannot describe the sulmazole plasma

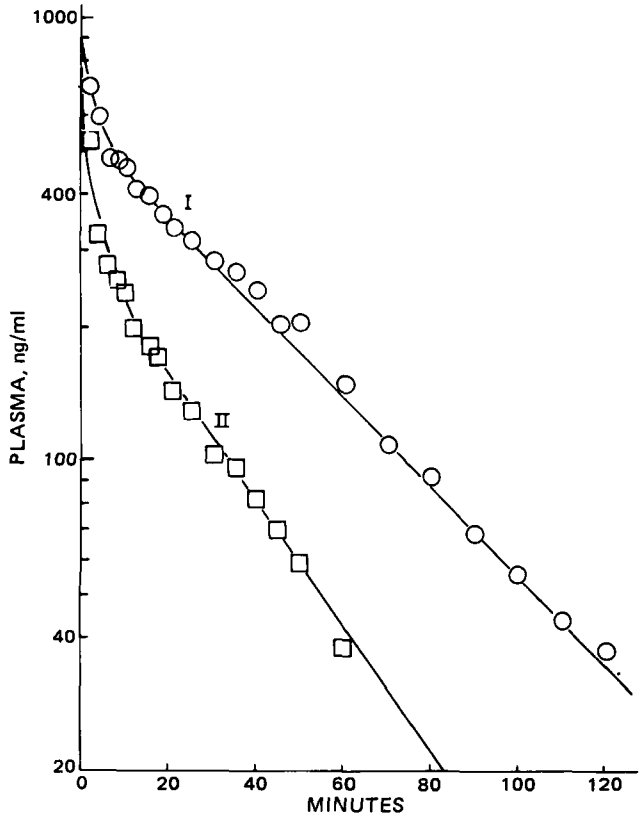

Figure 4—*Semilogarithmic plots of plasma levels of sulmazole (I) and II after intravenous administration of 0.7 mg/kg of each to dog 1. The curves through the data were constructed from the parameters given in Table II in accordance with* $p = ae^{-\alpha t} + be^{-\beta t}$.

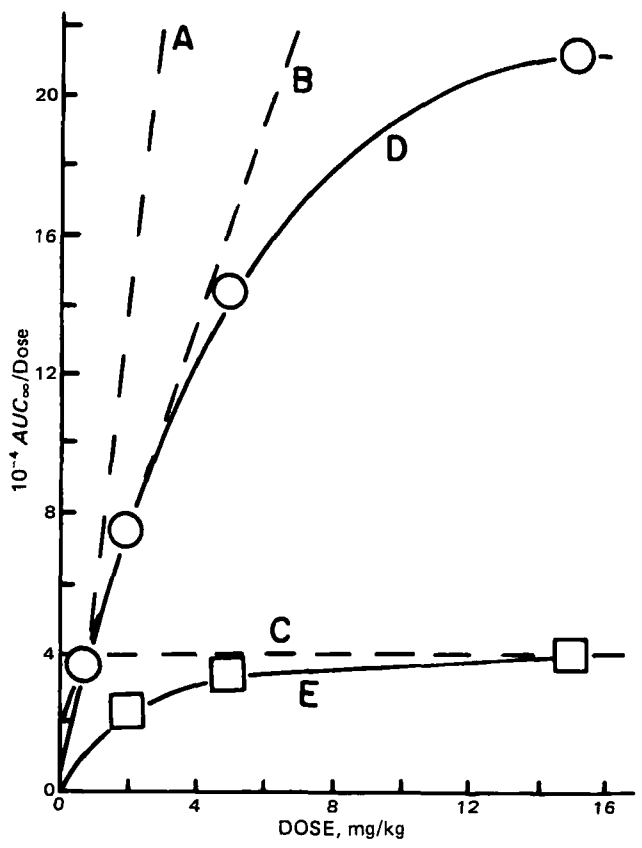

Figure 5—*Plots of ratios of total area under the curve (ng/min/ml^{-1}) to dose (mg/kg) against dose for sulmazole (○), curve D, and metabolite II (□), curve E. The anticipated forms of curves expected are given as dashed lines for (A) zero-order kinetics with constant elimination rates at all doses, (B) saturable pharmacokinetics with constant Michaelis–Menten parameters at all doses, and (C) first-order elimination rates.*

level–time data at all doses, even though it may give a reasonable fit at a given dose. The linearities of the plasma level–time data (Fig. 3) over such long time periods deny the existence of significant parallel first-order processes of elimination. Such processes could increase elimination rates at higher doses and plasma concentrations.

The apparent zero-order rate constants, k_0^I/V_I (ng/ml/min) in the 2–15-mg/kg dose range can be well characterized by the linear plot of their average values *versus* dose of sulmazole (mg/kg), $r = 0.9996$, to give:

$$k_0^I/V_I(\pm 0.26) = 0.985(\pm 0.027) \times \text{Dose} + 4.17 \pm 0.25 \quad \text{(Eq. 7)}$$

The apparent overall volumes of distribution referenced to plasma concentration of sulmazole apparently were dose independent and were obtained from the intercept, C_0, obtained from the extrapolation of the *straight line* of best fit through the plasma level–time data and averaged V_I = dose (ng)/C_0 (ng/liter) = 36.5 ± 1.7 liters. The value of V_I by this method was 30 liters for the 0.7-mg/kg dose (Table II, Fig. 4). These volumes could also be estimated from the intercept, C_0', obtained from extrapolation of the plateau in the 40–100-min interval (Fig. 3) after intravenous administration and a V_I' = dose (ng)/C_0' (ng/liter) = 41.0 ± 1.1 liters. The latter equation may be the more valid estimate if enterohepatic circulation did exist. Its existence would cause an overestimation of C_0 in the equilibrated fluids of the body and an underestimation of the apparent volume of distribution by the former method. The lower standard error of the mean of the latter (V_I') with respect to the former (V_I) at several doses confirms this. The values are listed in Table I. The averages of the $(k_0^I)' = V_I'(k_0/V_I)$ of sulmazole eliminated from the body are correlated well with the dose in milligrams per kilogram in the 2–15-mg/kg range, $r = 0.9982$, by:

$$k_0^I \pm 0.161 = (0.426 \pm 0.167) \times \text{Dose} + 1.71 \pm 0.15 \quad \text{(Eq. 8)}$$

Areas Under Plasma Sulmazole Level–Time Curves and Possible Relations to Doses—The total area under the plasma level–time curve for saturable (Michaelis–Menten) disposition pharmacokinetics for the one-compartment body model (23) of volume V with an intravenous bolus is:

$$AUC_\infty^{sat} = \frac{D}{v_{max}V}\left(\frac{D}{2V} + K_m\right) = \frac{D}{k_0}\left(\frac{D}{2V} + K_m\right) \quad \text{(Eq. 9)}$$

Thus:

$$AUC_\infty^{sat} = \frac{D^2}{2v_{max}V^2} + \frac{K_mD}{v_{max}V} = \frac{D^2}{2k_0V} + \frac{K_mD}{k_0} \quad \text{(Eq. 10)}$$

The ratio of the total area under the plasma level–time curve for zero-order elimination (k_0) to dose (D) for the one-compartment body model with an intravenous bolus is:

$$\frac{AUC_\infty^0}{D} = \frac{D}{2v_{max}V^2} = \frac{D}{2k_0V} \quad \text{(Eq. 11)}$$

where $v_{max} = k_0/V$.

In Eqs. 10 and 11 plots of the ratio of total area–dose should be linear functions of dose with a positive slope. In the saturable case (Eq. 10), the intercept should be positive; in the zero-order case (Eq. 11), the intercept should be zero.

The ratio of the total AUC for first-order elimination to the doses is a constant:

$$AUC_\infty^I/D = 1/\beta V = 1/Cl_{tot} \quad \text{(Eq. 12)}$$

where the total clearance (Cl_{tot}) is a product of the terminal rate constant (β) and the apparent overall volume of distribution (V).

Such ratios of AUC–dose in milligrams per kilogram are given in Table I for sulmazole, AUC_∞^I/D. The ratio for the 0.7-mg/kg dose was 36,000. A plot of the ratio *versus* dose is given in Fig. 5 for sulmazole. The ratio increases with dose to indicate nonlinear pharmacokinetics, but it does not increase linearly. Sulmazole does not conform to the patterns anticipated for true saturable or zero-order pharmacokinetics in the one-compartment body model. This is a consequence of the apparent increases of v_{max} or k_0^I/V (Fig. 3, Table I) with the initial dose, where k_0^I/V, the zero-order rate of elimination, persists throughout the major time course of the drug in the plasma.

Pharmacokinetics of the Formation of II from Sulmazole—The time courses of formation of II in the plasma on intravenous administration of sulmazole at 2, 5, and 15 mg/kg are plotted in Fig. 6 for the

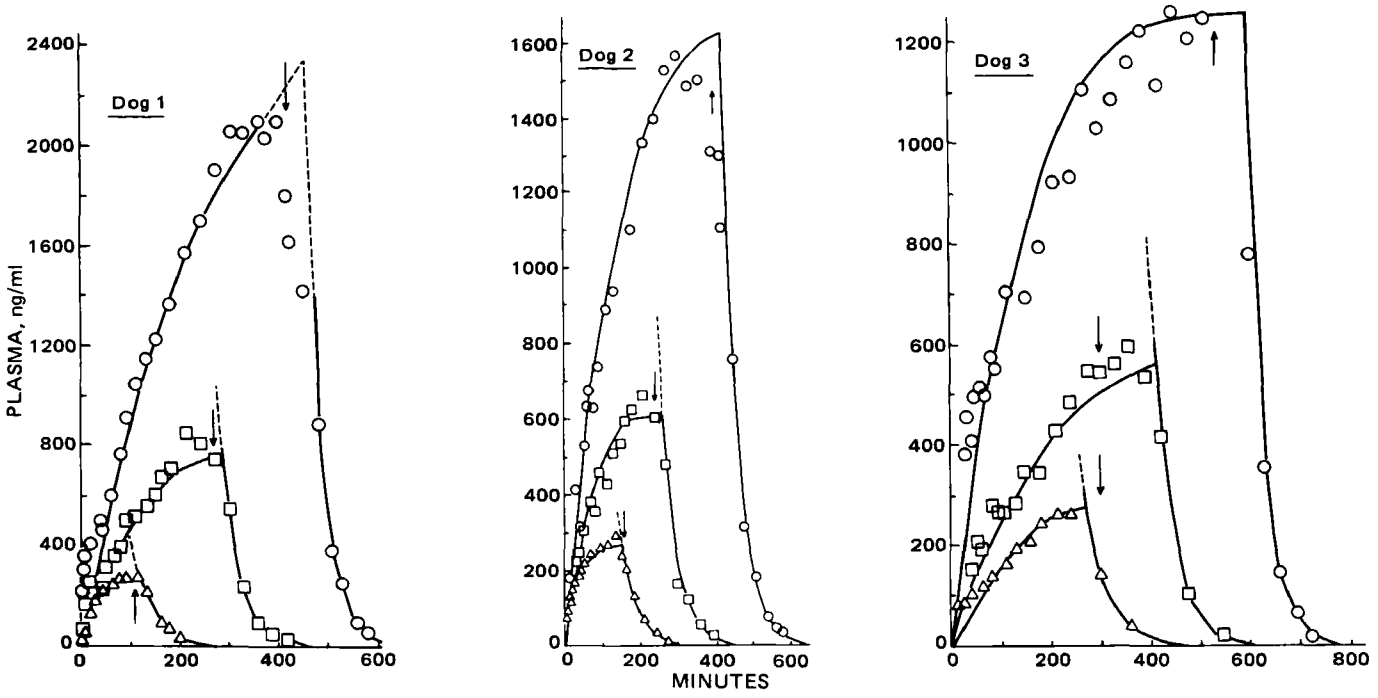

Figure 6—*Linear plots of plasma levels of metabolite II as formed with time after intravenous administration of 2 (△), 5 (□), and 15 (○) mg/kg of sulmazole to dogs 1–3. The arrows designate the approximate times of cessation of zero-order depletion of sulmazole in the plasma. The curves drawn through the points prior to the maxima were calculated from [II] = $(k_0^{II}/V_{II})t - (Cl^{II}/V_{II})AUC_{II}$. The curves drawn through the points subsequent to the maxima were calculated from $C_0^{II}e^{-\beta_{II}t}$ where the pertinent parameters are given in Table I.*

studies in dogs 1, 2, and 3. The shapes of the curves imply a zero-order formation of II up to the times marked by the arrows, where sulmazole was depleted from the plasma and a subsequent first-order elimination. This hypothesis was challenged.

If first-order formation and elimination existed, the amount of II formed could be expressed as:

$$II = Cl^{I\to II}AUC^{I} - Cl^{II}AUC^{II} \qquad \text{(Eq. 13)}$$

where AUC^{I} and AUC^{II} are the respective areas under plasma level–time curves for I and II, and $Cl^{I\to II}$ and Cl^{II} are the clearances of I–II and of II, respectively. Since the amount of II = V_{II} [II], where V_{II} is the apparent overall volume of distribution of II, and [II] is the plasma level, Eq. 13 can be rearranged to:

$$[II]/AUC^{I} = Cl^{I\to II}/V_{II} - (Cl^{II}/V_{II})AUC^{II}/AUC^{I} \qquad \text{(Eq. 14)}$$

However, plots of the ratio of the plasma level [II] at a time t to the area under the plasma sulmazole–time curve up to that time t (AUC^{I}) against the ratio of the areas of plasma metabolite–time to plasma sulmazole–time (AUC^{II}/AUC^{I}) were decidedly nonlinear, contraindicating the validity of the postulation of first-order formation of II from sulmazole with a constant clearance $Cl^{I\to II}$ with subsequent first-order elimination or constant clearance of II, Cl^{II}.

A zero-order formation of the amount of II from sulmazole with subsequent first-order elimination can be expressed as:

$$II = k_0^{II}t - Cl^{II}AUC^{II} \qquad \text{(Eq. 15)}$$

This expression can be rearranged to:

$$[II]/AUC^{II} = (k_0^{II}/V_{II})(t/AUC^{II}) - Cl^{II}/V_{II} \qquad \text{(Eq. 16)}$$

and plots of the ratio of plasma levels of the metabolite [II] at a given time (t) to that of the area under the plasma metabolite concentration (AUC^{II}) to that time against the ratio of the time (t) to the AUC^{II} should be linear with a slope k_0^{II}/V_{II} (ng/ml/min) and a negative intercept of Cl^{II}/V_{II} (min^{-1}), the apparent overall rate constant of elimination of the metabolite from its equilibrated tissues. These plots (Fig. 7) were linear to confirming the postulation of zero-order formation of the metabolite, II, with its subsequent first-order elimination. The obtained zero-order rates of formation of II from sulmazole, k_0^{II}/V_{II} (ng/ml/min), and the apparent clearance per unit volume of II, Cl^{II}/V_{II} (min^{-1}), are given in Table I.

The plasma values of II with time were calculated with these parameters and plotted as the curves through the data before the maximal values in Fig. 6. The values of maximum time corresponded to the cessation times of the zero-order rate of depletion of sulmazole in the plasma (Figs. 3 and 4).

Subsequent to the maximal values, metabolite plasma levels of II decreased by an apparent first-order process which could be characterized by:

$$[II] = C_0^{II}e^{-\beta II t} \qquad \text{(Eq. 17)}$$

where the values for C_0^{II}, the apparent plasma level extrapolated to zero time, and β_{II}, the apparent overall first-order elimination rate constant of II, are listed in Table I. These latter values appear to be dose-independent for plasma concentrations <2000 ng/ml of II, and the half-lives average 26.5 ± 1.2 min, consistent with the terminal half-life of 21.2 min when 0.7 mg/kg of II was administered (Fig. 4, Table II), a dose when the pharmacokinetics of II appear to conform to a two-compartment body model with first-order processes. The plasma values of II on sulmazole administration, subsequent to the maximal values, were calculated from the obtained C_0^{II} and β_{II}-values of Table I and were plotted through the experimental data in Fig. 6.

The rate of appearance of II (ng/min), k_0^{II}, was calculated from the product of the k_0^{II}/V_{II}-values (Table I) and the apparent overall volume of distribution, V_{II} = 48,558 ml, obtained from the administration of 0.7 mg/kg iv of II (Table II). Although the k_0^{II}-values of II appearance decreased consistently (5.07 ± 0.31–2.89 ± 0.73 ng/min) with the decrease of sulmazole dose from 15 to 5 mg/kg, the values at 2 mg/kg of sulmazole were high for dogs 1 and 2 (>1). A possible reason is that the volume of distribution for II (V_{II}) obtained from the single 0.7-mg/kg iv bolus study of II and used to convert k_0^{II}/V_{II}, the zero-order rate of II appearance per unit of volume, to k_0^{II} was not valid in these particular studies. If these values were not included, the ratio of k_0^{II} (corrected to sulmazole equivalents) to k_0^{I}, the apparent zero-order rates of II appearance and sulmazole disappearance, respectively, averaged 0.75 ± 0.04 (Table I) and were reasonably consistent among doses and dogs. The two anomalous values at 2 mg/kg for dogs 1 and 2 showed ratios of 1.77 and 1.87, respectively. It is concluded that 75% of the sulmazole is transformed to its major metabolite, II, by the zero-order process, 73 ± 3% at 15 mg/kg and 81 ± 6% at 5 mg/kg of sulmazole.

If, as shown in Table I, a relatively constant fraction of II was formed from I and if II were eliminated only by first-order processes or dose-independent clearances, the ratio of the area under the plasma level–time curve for II to the dose would not change with dose in accordance with Eq. 12. The fact that there is an increase of the ratio AUC_{∞}^{II}/dose with dose (Table I, Fig. 5), although not as significantly great as the comparable

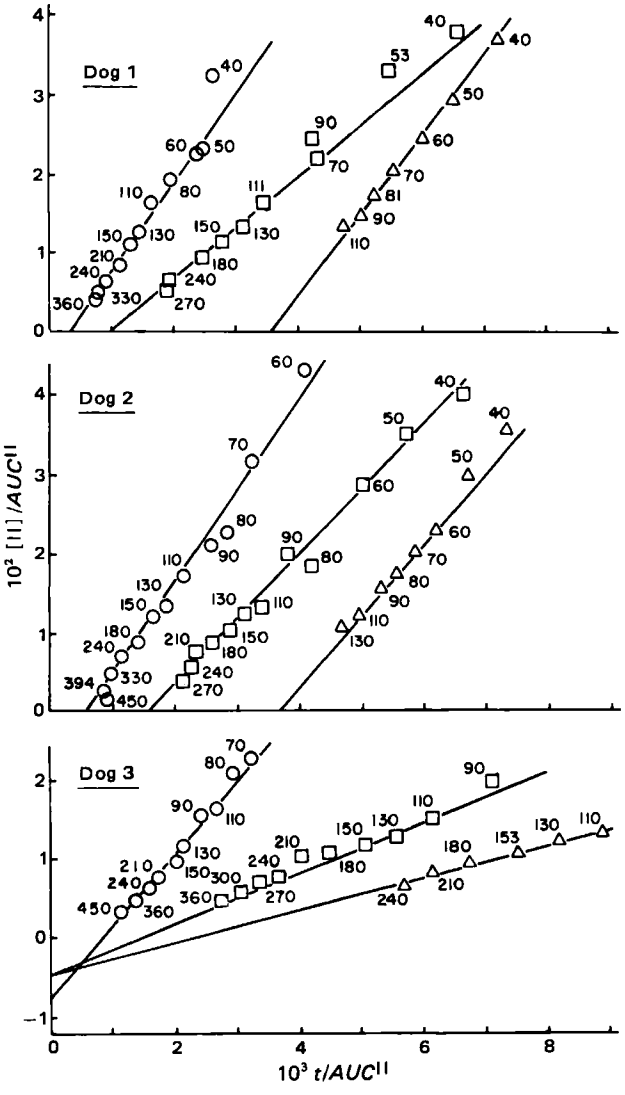

Figure 7—*Plots in accordance with Eq. 16 for the estimation of the zero-order appearance of metabolite II (slope = k_0^{II}/V_{II}, ng/ml/min^{-1}) and its first-order disappearance (intercept = $-Cl^{II}/V_{II}$, min^{-1}) for intravenous doses of 2 (△), 5 (□), and 15 (○) mg/kg of sulmazole.*

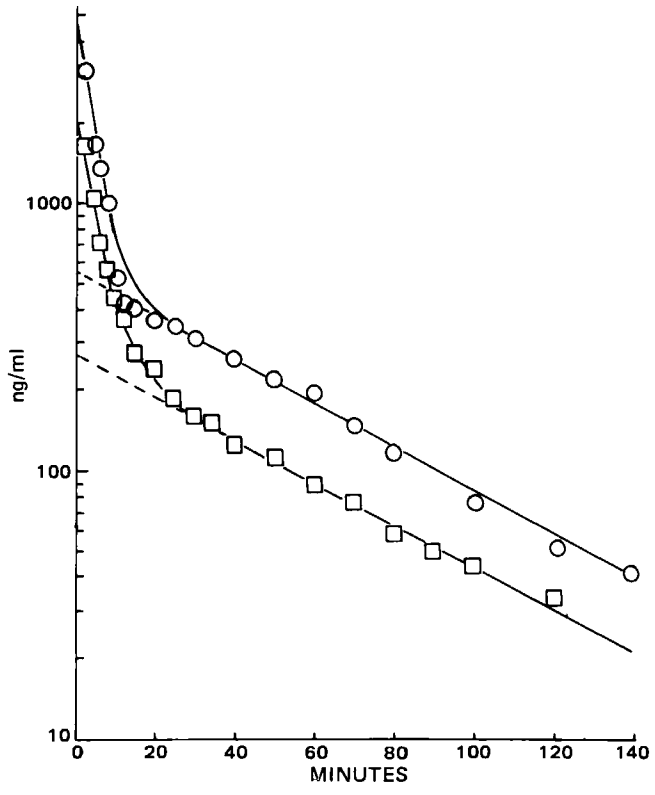

Figure 8—*Semilogarithmic plots of plasma levels of metabolite III against time when III was administered intravenously at 1 (□) and 2 (○) mg/kg. The curves through the data are drawn in accordance to* $p = ae^{-\alpha t} + be^{-\beta t}$ *where the pharmacokinetic parameters are given in Table II.*

ratio for sulmazole, indicates some degree of nonlinear pharmacokinetics for II at the higher sulmazole doses.

Pharmacokinetics of III—There was negligible renal excretion of unchanged I, II, and III. A possible route of metabolism of sulmazole, in addition to its oxidation to II, is its hydroxylation to III, since III is observed in the urine, although plasma III levels, even at 15 mg/kg of sulmazole, were below the analytical sensitivities.

The pharmacokinetics of III were studied at 1.0 and 2.0 mg/kg after intravenous administration of III and conformed to a two-compartment body model with apparent first-order transferences (Table II, Fig. 8). There were no apparent dose dependencies. Total clearances (1040 ml/min), terminal half-lives (37.3 min), and volumes of the central compartment (10 liters) and overall volumes (56 liters) were not significantly different for the two doses.

The lack of significant plasma levels and the fact that a week-long phenobarbital regimen did not increase sulmazole elimination rates significantly over the prephenobarbital regimen study at a dose of 2 mg/kg of sulmazole (Fig. 1) indicates that the hydroxylated compound is not a major product in sulmazole elimination. Phenobarbital is a well-known inducer of phenyl ring hydroxylation.

Renal Elimination of I and Metabolite II—Unchanged I was excreted renally at an average of 2.3 ± 0.4% of the administered dose (Table III) with no apparent statistically significant dose effects. Similarly, an average of 0.27 ± 0.05% of the administered sulmazole dose was excreted renally as metabolite II. Typical plots of cumulative amounts excreted with time are given in Fig. 9.

When there were narrow ranges of urine flow rates (Table III) reasonably constant renal clearances could be obtained from the regressions:

$$\Delta U/\Delta t = Cl_{ren} p_{t_{mid}} \quad \text{(Eq. 18)}$$

where $\Delta U/\Delta t$ is the amount (ΔU) of material excreted in a time interval (Δt), where $p_{t_{mid}}$ is the plasma level at the mid time of that interval, and:

$$\Sigma U = Cl_{ren} AUC \quad \text{(Eq. 19)}$$

where ΣU is the cumulative amount of material excreted at a time when AUC is the area under the plasma level–time curve up to that time.

In those cases where the urine flow rates varied over wider ranges, it was not possible to obtain reasonable correlations for Eqs. 18 and 19. The apparent renal clearance (Cl_{ren}^{app}) showed significant functional dependence on urine flow rate ($\Delta V/\Delta t$):

$$Cl_{ren}^{app} = (\Delta U/\Delta t)/p_{t_{mid}} = a \pm s_a + (b \pm s_b)(\Delta V/\Delta t) \quad \text{(Eq. 20)}$$

Examples of this dependence are shown in Fig. 10. Fittings of cumulative amounts of materials excreted into the urine with time are shown in Fig. 9 for the premises of constant renal clearance and renal clearances varying with urine flow rates using the parameters of Eq. 20 listed in Table III.

The apparent renal clearances of sulmazole varied between 1.6 and 7.4, except for the 13.8 ml/min of the 0.7-mg/kg dose with an overall average of 3.9 ± 0.8 ml/min. The apparent renal clearance of metabolite II varied between 1.0 and 3.4 ml/min, except for the 6.4 ml/min from the 0.7-mg/kg dose of sulmazole, with an overall average of 1.8 ± 0.3 ml/min. Even when corrected for protein binding, the respective renal clearance referenced to free drug in plasma of I and II did not exceed 6.6 and 3.91 ml/min. This is strong evidence for a high excess of tubular reabsorption which is supported by the dependence of apparent renal clearance on urine flow rate (Eq. 20).

The renal clearance of 0.7 mg/kg of intravenously administered II was 3.0 ml/min from the plot in accordance with Eq. 18 (Fig. 11). The renal clearance of 1.0 and 2.0 mg/kg of intravenously administered III was independent of dose (0.25 ml/min) (Fig. 11). The plots of cumulative urinary excretion against time of III are given in Fig. 12 and conformed to the values calculated in accordance with Eq. 19.

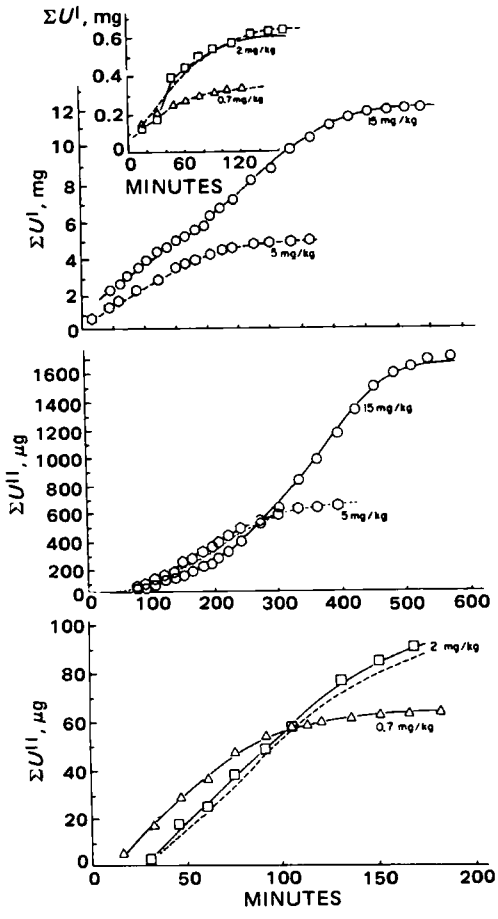

Figure 9—*Plots of cumulative amounts of unchanged sulmazole and metabolite II excreted in urine for the labeled amounts of sulmazole administered intravenously to dog 1. The dashed lines are plotted for an assumed sulmazole constant renal clearance, Cl^{I}_{ren}, of 7.4, 7.77, and 13.8 ml/min for the 5-, 2-, and 0.7-mg/kg doses, respectively, in accordance with $\Sigma U^{I} = Cl^{I}_{ren} AUC^{I}$. Dashed lines are plotted for an assumed metabolite II constant renal clearance, Cl^{II}_{ren}, of 3.35 and 2.77 ml/min for the sulmazole doses of 5 and 2 mg/kg, respectively, in accordance with $\Sigma U^{II} = Cl^{II}_{ren} AUC^{II}$. The solid lines are calculated for a urine flow-dependent renal clearance, $Cl_{ren} = a + b(\Delta V/\Delta t)$ where the a and b constants are given in Table III.*

Possible Rationales for the Unusual Nonlinear Pharmacokinetics of Sulmazole—The higher maximal zero-order rates of sulmazole elimination and transformation over large sulmazole concentration ranges at higher initial doses of sulmazole cannot be described by simple Michaelis–Menten kinetics. It is possible to speculate why. The hypothesis of product-inhibited processes (as by hydroxylated metabolite) (25) cannot explain this phenomenon, since this factor would lower maximal zero-order rates with the higher dose. In addition, it has been shown that *p*-hydroxylation of the phenyl ring is not the major metabolic route.

It was recently argued (25) that the Michaelis–Menten model for nonlinear processes has definite limitations, in that its basic premise is the establishment of a quasi-equilibrium process; *i.e.*, the validity of Eq. 1 is based on the premise of ready establishment of an equilibrium between the drug and the metabolizing enzyme where the subsequent rate-determining step depends on the concentrations of enzyme-bound substrate. A general unsteady-state model was proposed which denies the steady-state postulate underlying Michaelis–Menten kinetics. These concepts were applied to the simulation of plasma level–time curves on the premise of competition of metabolic products with substrate for plasma-, enzymes-, and tissue-binding sites to demonstrate that product-inhibited transformations would not necessarily conform to Michaelis–Menten kinetics.

The unsteady state concept may be useful to model this system, where the apparent zero-order elimination rate of sulmazole disappearance and metabolite II appearance seems to be dose- and initial plasma concentration-dependent. Speculation on the basis of an unsteady state possibly could lead to explanations of the unusual nonlinear pharmacokinetics

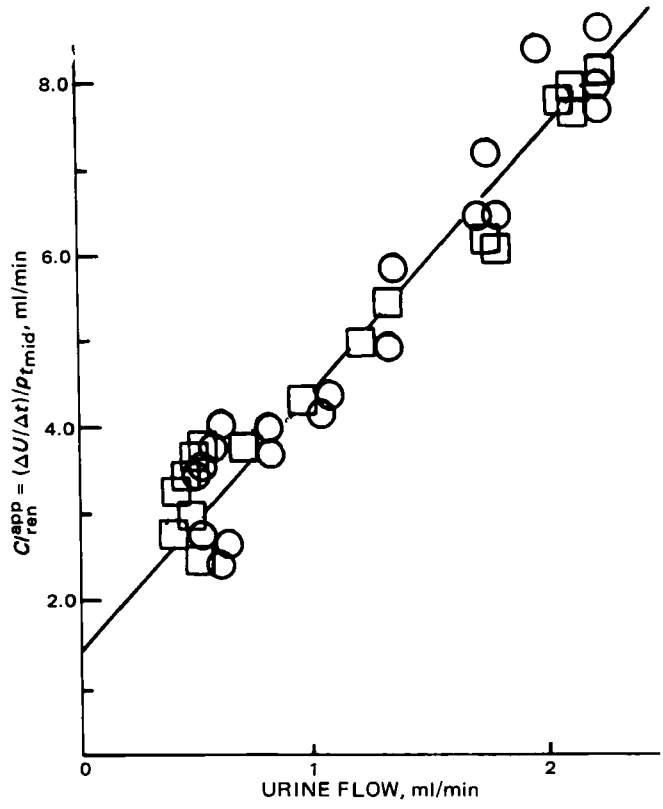

Figure 10—*Example of the dependence of the apparent renal clearance, Cl^{app}_{ren}, of sulmazole (○) and II (□) for a urine collection interval on the urine flow rate, $\Delta V/\Delta t$, in that interval for dog 1 (15-mg/kg dose study).*

of sulmazole where the major route of sulmazole substrate metabolism to II can be postulated as:

$$S + R \underset{k_2}{\overset{k_1}{\rightleftharpoons}} (SR) \xrightarrow{k_3} (MR) \xrightarrow{k_4} M + R \qquad \text{(Eq. 21)}$$

and it can be conjectured that substrate (S) has noninstantaneous but high affinity to large numbers (R) of receptor sites.

If the rate of transformation of receptor-bound substrate (SR) to receptor-bound metabolite (RM) and the subsequent regeneration of free receptor sites by dissociation of metabolite (M) were not instantaneous processes, there could be a preliminary interval when few free receptor sites would be available to bind to the substrate. This would explain the existence of initial plateaus in the plasma level–time curves of Fig. 3 subsequent to an initial drop in plasma levels and provide an alternative explanation to enterohepatic circulation as their cause.

Also, if the transformation of receptor-bound substrate (SR) to receptor-bound metabolite (RM) and its subsequent dissociation were rate-determining and time-dependent processes, the release of receptor-bound metabolite and the removal of substrate by available receptor sites would be greater for initially higher doses (or concentrations) of

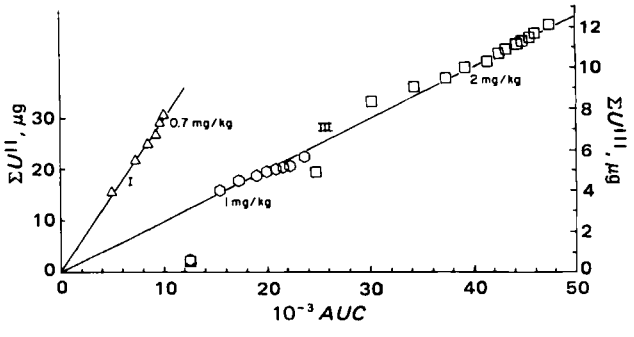

Figure 11—*Renal clearance plots in accordance with Eq. 19 for intravenous administration to dog 1 of 0.7 mg/kg of II (△, left ordinate, Cl^{II}_{ren} = 3.0 ml/min) and 1.0 (□) and 2.0 (○) mg/kg of III (right ordinate, Cl^{III}_{ren} = 0.25 ml/min).*

Table III—Parameters of Renal Elimination of Sulmazole and Metabolite II on Intravenous Administration of Sulmazole

Dog	mg/kg	ΣU_∞, mg I	ΣU_∞, mg II	Dose, %[a] I	Dose, %[a] II	Estimated Average Renal Clearances, ml/min: ΣU versus AUC[b] I	ΣU versus AUC[b] II	$\Delta U/\Delta t$ versus $p_{t_{mid}}$[c] I	$\Delta U/\Delta t$ versus $p_{t_{mid}}$[c] II
	15	12.0	1.686	3.6	0.48	—[d]	—[d]	—[d]	—[d]
	5	4.8	0.602	3.8	0.45	7.4 ± 0.1	2.4 ± 0.1	7.3 ± 0.4	3.4 ± 0.6
1	2	0.64	0.091	1.4	0.18	6.4 ± 0.3	2.8 ± 0.1	5.2 ± 0.9	—[d]
	0.7	0.34	0.065	2.0	0.36	13.8 ± 0.16	6.4 ± 0.4	—[d]	—[d]
	15	5.4	0.501	1.4	0.13	1.6 ± 0.1	1.2 ± 0.2	—[d]	—[d]
2	5	1.5	0.195	1.2	0.15	2.0 ± 0.1	—[d]	—[d]	1.0 ± 0.2
	2	0.32	0.048	0.65	0.10	1.6 ± 0.2	1.2 ± 0.1	1.9 ± 0.1	—[d]
	15	14.2	1.586	3.6	0.38	4.5 ± 0.1	1.8 ± 0.2	—[d]	1.4 ± 0.7
3	5	5.4	0.403	4.3	0.31	5.9 ± 0.2	2.1 ± 0.1	4.3 ± 0.9	2.3 ± 0.4
	2	0.52	0.062	1.0	0.11	2.2 ± 0.1	1.0 ± 0.1	2.0 ± 0.2	1.2 ± 0.1

Dog	mg/kg	$a + s_a$[e] I	$a + s_a$[e] II	$b + s_b$[e] I	$b + s_b$[e] II	r[g] I	r[g] II	Urine Flow, ml/min
	15	1.27 ± 0.22	0.8 ± 0.2	3.1 ± 0.2	1.2 ± 0.1	0.97	0.90	0.5–2.5
1	5	—[f]	1.7 ± 0.3	—[f]	1.4 ± 0.2	—[f]	0.85	0.6–2.4
	2	0.7 ± 2.1	−0.9 ● 0.3	3.8 ± 1.5	2.6 ± 0.2	0.72	0.98	0.6–2.0
	0.7	5.4 ± 3.0	0.1 ± 0.1	4.7 ± 0.7	3.4 ± 0.4	0.94	0.97	0.7–3.0
	15	0.5 ± 0.1	−0.1 ± 0.1	2.7 ± 0.4	0.6 ± 0.1	0.97	0.93	0.3–2.0
2	5	0.4 ± 0.3	0.0 ± 0.3	2.5 ± 0.4	1.9 ± 0.3	0.87	0.85	0.3–0.8
	2	—[f]	—[f]	—[f]	—[f]	—[f]	—[f]	0.4–0.7
	15	—[f]	—[f]	—[f]	—[f]	—[f]	—[f]	0.4–0.6
3	5	2.2 ± 0.3	0.8 ± 0.1	3.2 ± 0.3	1.5 ± 0.1	0.95	0.93	0.3–2.0
	2	—[f]	—[f]	—[f]	—[f]	—[f]	—[f]	0.1–0.3

[a] $100 \times \Sigma U_\infty$/dose (mg) where ΣU^{II} is converted to weight equivalents of I, *i.e.*, multiplied by mol. wt. I/mol. wt. II = 0.95. [b] Regression coefficient and its standard error of estimate for plots of cumulative amount excreted against the area under the plasma level–time curve for the respective compound at the time of cumulative excretion. [c] Regression coefficient and its standard error of estimate for plots of rate of excretion in an interval against the plasma level at the midtime of that interval. [d] Specified plots were nonlinear due to Cl_{ren} dependence on urine flow. [e] Constants for the linear regression and their standard errors (22) of apparent renal clearances [$Cl_{ren} = (\Delta U/\Delta t)/p_{t_{mid}}$ (ml/min)], the ratio of amount of compound excreted in a time interval, Δt, divided by the plasma level of compound at the midtime of that interval, on the urine flow rate [$\Delta V/\Delta t$, ml urine/the collection interval (ml/min)] in accordance with $Cl_{ren} = (b \pm s_b)(\Delta V/\Delta t) + a \pm s_a$. [f] Insufficient variation in urine flow ($\Delta V/\Delta t$) to warrant attempted regression of Cl_{ren} or no significant regression. [g] Correlation coefficient for dependence of apparent renal clearance on urine flow rate.

sulmazole when the plasma levels reach those initially obtained from lower doses than when the lower doses were administered. Thus, a dose-dependent rate of loss of sulmazole would be observed, since there would be slower overall rates of metabolism at lower doses where the available sites would be occupied by metabolites for greater fractions of the time course and not available for the depletion of plasma levels.

This model has been confirmed by simulation on the analogue computer. The conformity of the simulations with the observed data will be presented in detail in the future.

Summary—The experimental data indicate that the higher dose and initial concentration give the greater constant rate of sulmazole loss from plasma. The proposed nonsteady-state model would account for these unusual nonlinear pharmacokinetics if it is speculated that all receptor sites can be potentially occupied by substrate, but not instantaneously, that there is a time- and plasma concentration-dependent rate of occupation of receptor sites and a time-dependent release of metabolite to provide unreacted receptor sites.

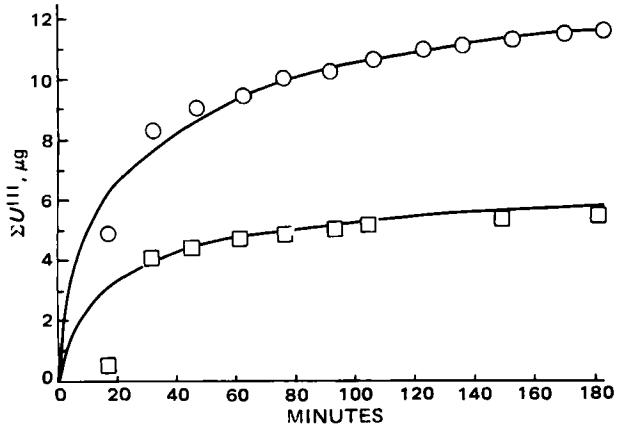

Figure 12—*Cumulative plots of III excreted with time at 1.0 (□) and 2.0 (○) mg/kg iv of III administered to dog 1. The curves drawn through the data were plotted in accordance with* $\Sigma U^{III} = Cl^{III}_{ren}AUC$ *where* $Cl^{III}_{ren} = 0.25$ *ml/min.*

An alternative explanation can be based on the hypothesis that high concentrations of sulmazole, metabolite II, and/or another metabolite can cause an irreversible, allotropic modification of the receptor so that binding of substrate, transformation to metabolite, and/or release of metabolite are enhanced.

REFERENCES

(1) W. Diederen and R. Kadatz, *Arzneim.-Forsch. (Drug Res.)*, **31**, 146 (1981).

(2) J. Dämmgen, R. Kadatz, and W. Diederen, *ibid.*, **31**, 151 (1981).

(3) G. Hellige, D. Baller, F. B. M. Ensick, J. Zipfel, H. G. W. Wolpers, and H. J. Bretschneider, *ibid.*, **31**, 155 (1981).

(4) Th. Hockerts, B. Höcht, R. Broll, K. Trenkel, J. Sieber, A. Kilian, and B. Brendle, *ibid.*, **31**, 157 (1981).

(5) L. Benedikter and T. Mey, *ibid.*, **31**, 239 (1981).

(6) G. F. Hauf, P. Bubenheimer, and H. Roskamm, *ibid.*, **31**, 253 (1981).

(7) H. Drexler, H. Wollschläger, H. Löllgen, and H. Just, *ibid.*, **31**, 259 (1981).

(8) M. Stauch and W. Nechwatal, *ibid.*, **31**, 267 (1981).

(9) K. D. Ruffmann, H. C. Mehmel and W. Kübler, *ibid.*, **31**, 271 (1981).

(10) J. Thormann, W. Kramer,and M. Schlepper, *ibid.*, **31**, 273 (1981).

(11) U. Busch, *ibid.*, **31**, 204 (1981).

(12) *Idem.*, **31**, 209 (1981).

(13) B. D. Cameron, G. H. Draffan, J. P. Dunsire, and A. Zimmer, Arneim.-Forsch. (Drug Res.), **31**, 217 (1981).

(14) A. Zimmer and R. Hammer, *ibid.*, **31**, 212 (1981).

(15) J. Mierau, *ibid.*, **31**, 221 (1981).

(16) W. Roth, A. Prox, A. Reuter, J. Schmid, A. Zimmer, and H. Zipp, *ibid.*, **31**, 232 (1981).

(17) W. Roth, A. Zimmer, and U. Busch, *ibid.*, **31**, 236 (1981).

(18) W. Roth, K. Beschke, R. Jauch, A. Zimmer, and F. W. Koss, *J. Chromatogr. Biomed. Appl.*, **222**, 13 (1981).

(19) H. Zipp, W. Roth, and A. Zimmer, *Arzneim.-Forsch. (Drug Res.)*, **31**, 200 (1981).
(20) P. H. Hinderling, J. Bres, and E. R. Garrett, *J. Pharm. Sci.*, **63**, 1684 (1974).
(21) E. R. Garrett and H. J. Lambert, *ibid.*, **62**, 550 (1973).
(22) HP-65, STAT-PAC-1 "Linear Regression," Hewlett-Packard, Corvallis, Ore., p. 49.
(23) E. R. Garrett, J. Bres, Kurt Schnelle, and L. L. Rolf, Jr., *J. Pharmacokinet. Biopharm.*, **2**, 43 (1974).
(24) J. G. Wagner, *ibid.*, **1**, 103 (1973).
(25) M. T. Smith and T. C. Smith, *Eur. J. Clin. Pharmacol.*, **20**, 387 (1981).

ACKNOWLEDGMENTS

Supported in part by an unrestricted grant from Dr. Karl Thomae GmbH, Biberach, West Germany.

The technical assistance of Mrs. Kathleen Eberst was greatly appreciated as was the discussion with Dr. Paul Altmayer and his analogue and digital computer simulations.

Effect of Insulin and Dinoprostone on D-Glucose and 2-Deoxy-D-Glucose Uptake by Normal and Diabetic Rat Hepatocytes

A. B. BIKHAZI *x, H. M. NUBANI, and E. L. COE ‡

Received July 17, 1981, from the **Department of Physiology and the* ‡*Department of Biochemistry, Faculty of Medicine, American University of Beirut, Beirut, Lebanon.* Accepted for publication November 25, 1981.

Abstract □ Suspensions of deaggregated hepatocytes were prepared by a collagenase perfusion technique from livers of both normal rats and rats rendered diabetic by streptozocin treatment. Uptake of D-glucose and 2-deoxy-D-glucose was estimated by adding ^{14}C- or ^{3}H-labeled hexose to a stirring suspension of cells in Krebs–Henseleit buffer at 37°, separating the cells by rapid centrifugation, and measuring radioactivity in the packed cell pellet. Uptake, calculated after correction for entrapped extracellular fluid, includes any hexose bound to, transported into, or otherwise immobilized in the cells. High concentrations of glucose (5–20 m*M*) establish an intracellular–extracellular distribution ratio near 1.0 within 1 min, indicating a facilitated diffusion transport system. In contrast, a low level of glucose (71 n*M*) almost immediately (<15 sec) establishes ratios of between 3 and 4, which suggests a significant amount of glucose binding to cell membrane. Such binding would not be detected at the high glucose levels because of its small magnitude. Hepatocytes from diabetic rats exhibit a decrease in this apparent binding to ~60% of normal; preincubation with 0.1 IU/ml insulin increases this toward normal values, although it does not affect the binding by normal hepatocytes themselves. Preincubation with 0.1 μ*M* dinoprostone depresses glucose binding in cells from both normal and diabetic rats. A low concentration (1.2 n*M*) of 2-deoxy-D-glucose establishes even higher intracellular–extracellular distribution ratios of between 4 and 6, but the apparent binding of this sugar is identical in normal and diabetic rat hepatocytes and is not affected by preincubation with either insulin or dinoprostone alone. However, combined treatment with both agents causes a significant increase in 2-deoxyglucose binding. The results suggest that insulin promotes formation of hexose-binding sites and conversion of these to specific glucose-binding sites while dinoprostone may act by blocking the latter conversion.

Keyphrases □ Insulin—effect on D-glucose and 2-deoxy-D-glucose uptake, normal and diabetic rat hepatocytes, dinoprostone □ Dinoprostone—effect on D-glucose and 2-deoxy-D-glucose uptake, normal and diabetic rat hepatocytes, insulin □ Hepatocytes—rat, normal and diabetic, effect of insulin, dinoprostone on D-glucose, 2-deoxy-D-glucose uptake

The roles of insulin and prostaglandins on glucose retention by adipocytes, muscle cells, and hepatocytes have been the subject of contention in the literature. Although some have denied the existence of any stimulatory action of insulin on sugar retention by normal hepatocytes (1, 2), others have demonstrated an increase in liver glycogen deposition in response to this hormone (3, 4). Treatment of diabetic animals with insulin is reported to augment glucose uptake by liver (5, 6), and insulin may also enhance sugar uptake by adipocytes (7) and muscle cells (8, 9). Dinoprostone stimulates glucose uptake and oxidation by adipocytes (10) and intravenous infusion of dinoprostone in humans increases blood glucose levels (11). The present study demonstrates that insulin specifically enhances binding of low levels of glucose to hepatocytes and that dinoprostone inhibits this binding

EXPERIMENTAL

Preparation of Rat Hepatocytes—Liver parenchymal cells were isolated and prepared by the procedure of Bikhazi *et al.* (12), which modified procedures previously described by Berry and Friend (13) and Ingebretsen and Wagle (14).

Tests for Cell Viability—Trypan blue exclusion test for cellular viability was routinely performed before and after the experiments and preparations showing 90% viable cells or more were used.

The metabolic state of the hepatocytes during the incubation period was examined by following the respiration rate of cell suspensions in several separate experiments. Oxygen tension was recorded continuously with the aid of a biological oxygen monitor[1]. Rates were determined from the slopes of the oxygen tension curves and were calculated in terms of μl of oxygen/mg of cell protein. Protein was determined by the biuret reaction, using bovine serum albumin as a standard on centrifuged cell pellets dissolved in 1 *N* NaOH to minimize possible interference from medium components.

Preparation of Diabetic Rats—Rats were rendered diabetic by streptozocin treatment following the procedure of Chandramouli and Carter (15) as modified by Bikhazi *et al.* (12).

Isotopically Labeled Hexose—In all experiments with labeled glucose, 10 μCi of [1-^{14}C]D-glucose (58 mCi/mmole) was added to 226 ml of buffer to give a final concentration of 71 n*M*. In experiments with labeled 2-deoxyglucose, 5 μCi of [1-^{3}H]-2-deoxy-D-glucose (18.8 Ci/mmole) was added to the same volume to give a final concentration of 1.2 n*M*.

Determination of Hepatocyte Count and Mean Diameter—Hepatocyte count (1.2×10^8 cells per liver) and mean diameter (20 μm) were estimated by the procedure of Bikhazi *et al.* (12) using an automated counting machine[2].

Uptake of D-Glucose and 2-Deoxy-D-glucose by Hepatocytes—In general, 15×10^6 cells obtained from one rat liver were added to 225 ml of stirred Krebs–Henseleit solution in a water-jacketed beaker at 37° (the data in Tables I and II represent results from six different animals). After 45 min a small volume of isotopically labeled hexose was added, and 1.5 ml aliquots of suspension were periodically withdrawn, transferred to

[1] Yellow Springs Instruments, Yellow Springs, Ohio.
[2] Coulter Counter model A, Coulter Electronics, Hialeah, Fla.

0022-3549/83/0200-0116$01.00/0